Earth and Planetary Science Letters 341–344 (2012) 58–67

Contents lists available at SciVerse ScienceDirect

Earth and Planetary Science Letters

journal homepage: www.elsevier.com/locate/epsl

# Distribution of hydrous minerals in the subduction system beneath Mexico

YoungHee Kim *,[1], Robert W. Clayton, Jennifer M. Jackson

*Seismological Laboratory, Division of Geological and Planatery Sciences, California Institute of Technology, Pasadena, CA 91125, USA*

ARTICLE INFO

*Article history:*
Received 3 January 2012
Received in revised form
26 May 2012
Accepted 1 June 2012
Editor: P. Shearer
Available online 6 July 2012

*Keywords:*
subduction
Mexico
receiver function
hydrous minerals
Bayesian inversion

ABSTRACT

Teleseismic converted phases are used to probe the composition of the downgoing oceanic crust as a function of depth along the Cocos slab in central and southern Mexico. Previously, modeling of the receiver function (RF) conversion amplitude of the flat Cocos slab beneath central Mexico at 45 km depth revealed a thin low-velocity upper oceanic crust of a thickness of $4 \pm 1$ km, which has much lower seismic velocities ($\sim 20-30\%$ reduction in shear wave velocities) than (normal) lower crust. High Vp/Vs ratio ($\sim 2.0$) also suggested a large concentration of hydrous minerals such as talc in combination of high pore-fluid pressure in the horizontal segment. We extend this previous effort to examine seismic properties of both the steeply subducting Cocos oceanic crust beneath the Trans-Mexican Volcanic Belt (TMVB) in central Mexico and the shallowly dipping crust beneath southern Mexico. Inverted seismic velocities using the converted amplitudes at the top and bottom of the dipping oceanic crust are compared with experimentally constrained seismic velocities of candidate mineral phases in a range of likely pressures and temperatures. The composition of the oceanic crust downdip in the steep part of slab beneath the TMVB includes the minerals such as lawsonite and zoisite at 60–100 km depth, and the eclogitization occurs around 100 km depth. This is related to arc volcanism in the TMVB directly above the slab as well as the slab rollback. In contrast, the dominant mineral phase in the upper oceanic crust of southern Mexico beneath the Isthmus of Tehauntepec is amphibole on top of unaltered gabbroic oceanic crust. The difference in mineral assemblages of the subducted oceanic crust may help explain the difference in slab geometries between central and southern Mexico.

Published by Elsevier B.V.

## 1. Introduction

Hydrous minerals initially form within oceanic lithosphere as a result of hydrothermal circulation and alteration at spreading ridges, along fracture zones, and along faults in the region of the trench and outer rise (Maruyama and Okamoto, 2007; Audet et al., 2009). Such processes determine geophysical and mineralogical properties of the oceanic lithosphere with significant consequences for the mechanical behavior of subduction zones (Bach and Früh-Green, 2010). In particular, bending-related faulting affects porosity and permeability structure of the oceanic crust and consequently creates a pathway for fluids down to mantle depth (Ronero et al., 2003; Contreras-Reyes et al., 2007). However, there is little constraint on in situ abundance and distribution of hydration within subducting crust near the trench to fully assess the strength of the plate interface and nature of mega earthquakes. Also, experimental measurements of expected seismic wave speeds and anisotropy of the hydrous minerals in the subducted oceanic crust under different pressure and temperature conditions are limited, although significant progress has been made in recent years (e.g., Jacobsen and van der Lee, 2006). Knowledge of the material properties (seismic velocities and densities) of mineral phase assemblages along with appropriate phase equilibria are important in interpretation of geophysical observations and geodynamic simulations.

The presence of hydrous minerals in the oceanic crust reduces the seismic velocity to considerably less than the velocity of the surrounding mantle according to laboratory measurements on candidate phases (e.g., Jacobsen and van der Lee, 2006). As oceanic plates subduct, mineral-bound $H_2O$ is transported down into the deep mantle (Abers, 2000; Hacker et al., 2003b; Jacobsen and van der Lee, 2006; Maruyama and Okamoto, 2007; Mainprice and Ildefonse, 2009). The evidence has been seismically detected via tomography and receiver function (RF) based on teleseismic P-to-S converted (hereafter Ps) phases in various subduction environments as a low-velocity layer atop of the subducting plate (e.g, Alaska—Ferris et al., 2003, Cascadia—Nicholson et al., 2005; Abers et al., 2009; Audet et al., 2009; Peacock et al., 2011, central Andes—Yuan et al., 2000, southwest Japan—Shelly et al., 2006, northeast Japan—Kawakatsu and Watada, 2007; Tsuji et al., 2008, and central Mexico—Pérez-Campos et al., 2008; Kim et al., 2010).

* Corresponding author.
*E-mail addresses:* ykim@ldeo.columbia.edu (Y. Kim), clay@gps.caltech.edu (R.W. Clayton), jackson@gps.caltech.edu (J.M. Jackson).
[1] Now at Lamont-Doherty Earth Observatory, Columbia University, Palisades, NY 10964, USA.

0012-821X/$ - see front matter Published by Elsevier B.V.
http://dx.doi.org/10.1016/j.epsl.2012.06.001

Two above-mentioned seismic methods yield high P-to-S velocity ratio (Vp/Vs) exceeding 2.0 at the top interface of the subducting plate. In particular, a depth-section of RFs typically shows the oceanic crust as a dipping low-velocity layer, of which the top and bottom (plate interface and oceanic Moho) are outlined by strong negative and positive amplitudes, respectively. The estimates of the Vp/Vs by Audet et al. (2009) and Peacock et al. (2011) range between 2.0 and 2.4 in the shallowly dipping subducted oceanic crust beneath Vancouver Island from RFs. The timing of the reverberated phases from the top and bottom interfaces of the oceanic crust is used to constrain such high Vp/Vs of the downgoing crust (Audet et al., 2009). Abers et al. (2009) modeled and directly inverted RF waveforms, using a parameterization of structure with a few number of free parameters, and obtain Vp/Vs of 1.9 for the shallowly dipping Juan de Fuca crust beneath Washington, Cascades. Kim et al. (2010) performed an inversion using the amplitudes of the converted teleseismic phases and obtained high Vp/Vs of $\sim$2.0 within the flat upper oceanic crust of the Cocos plate beneath central Mexico. Furthermore, both finite-difference modeling of the RFs (Kim et al., 2010) and modeling local converted S-to-P phases and teleseismic underside reflections (Song et al., 2009) for the shallow-to-flat slab region ($\sim$20−45 km depth) suggested anomalously low S wave velocity of 2.4–3.4 km/s for 200 km from the Pacific coast.

In central Mexico, significant reduction in S wave velocity by more than 20% (Song et al., 2009) at the shallow-to-flat transition of the top interface of the Cocos plate ($\sim$20−45 km depth) are difficult to explain simply by velocity difference predicted for plausible subducted oceanic crust lithologies such as lawsonite blueschist and epidote blueschist (Currie et al., 2002), which is only less than 7% (Hacker et al., 2003a). In comparison to previously reported values for central Mexico subduction zone, the Vp/Vs ratios (or Poisson's ratios) shown in Audet et al. (2009) and Peacock et al. (2011) for Cascadia subduction zone are quite extreme, and both Audet et al. (2009) and Peacock et al. (2011) argued that such high estimates cannot be due to the presence of hydrous minerals alone but are due to free-water at high pore-pressure. This requires a very low permeability seal to retain the water. Kim et al. (2010) allowed for a compositional interpretation to explain such low-velocity anomalies at the depth of 20–45 km in central Mexico and suggested a large concentration of hydrous minerals such as talc and high pore-fluid pressure. In particular, low shear velocities in the shallowly dipping segment near the Pacific coast, which coincides with the transition zone downdip to the locked zone can be characterized by high seismic anisotropy (larger than 5%) with the foliation plane plunging $\sim$ 20° steeper than the plate interface of the Cocos plate with a dip angle of 18° (Song and Kim, 2012). This is consistent with crystallographic preferred orientation developed in S–C mylonites, and the talc could be pervasive near the top of the subducted oceanic crust (Song and Kim, 2012). The influence of the pore pressure on seismic velocities is, however, expected to diminish with depth (Christensen, 1984), and thus we expect that it is unlikely to be significant at lower oceanic crustal depths where the porosity is low and farther away from the seismogenic zone. It also needs very low viscosity to maintain a seal for over 200 km.

The evidence of high $H_2O$ content, bound in solid phases within the low-velocity layer, may explain the top (horizontal) interface of the Cocos plate in central Mexico which extends for 200 km from the Pacific coast without strong coupling between Cocos and North America plates (Kim et al., 2010). Plate decoupling, as shown in GPS observations (Franco et al., 2005), may explain the lack of seismicity and compression within the overriding plate in the last $\sim$20 Ma based on the tectonic and magmatic episodes in central Mexico (Nieto-Samaniego et al., 2006; Morán-Zenteno et al., 2007), despite the complete flat subduction geometry at shallow depth of 45 km (Pérez-Campos et al., 2008; Kim et al., 2010, 2012). Such large amount of fluid near the plate interface due to subduction related dehydration could also be an explanation for bursts of the nonvolcanic tremor within the subducted oceanic crust and lower continental crust (Payero et al., 2008) and slow slip events (Larson et al., 2007; Kostoglodov et al., 2010; Vergnolle et al., 2010; Radiguet et al., 2011). Recent studies suggest strong correlations between episodic tremor and slip (ETS) events and a low-velocity layer at the top of the subducting oceanic crust (Abers et al., 2009; Song et al., 2009; Audet et al., 2010; Kato et al., 2010).

In this study, we take an approach that Kim et al. (2010) used to constrain the seismic and mineralogical properties of the subduction interface using amplitudes of the converted phases and apply to regions where (1) the Cocos plate subducts steeply in central Mexico beneath active volcanic arc called Trans-Mexican Volcanic Belt (TMVB) and (2) the Cocos plate subducts shallowly beneath southern Mexico with the absence of volcanic arc in the Isthmus of Tehuantepec (Fig. 1). Our study region in central Mexico includes the portion where the seismic structure rapidly changes with depth due to slab bending and also largely covers the Quaternary Chichináutzin Volcanic Field, which is part of subduction-related arc and contains numerous cinder cones and shield volcanoes as well as larger stratovolcanoes such as the active Popocatépetl (Cervantes and Wallace, 2003; Johnson et al., 2009) (Fig. 1). On the basis of our inferred compositional models for

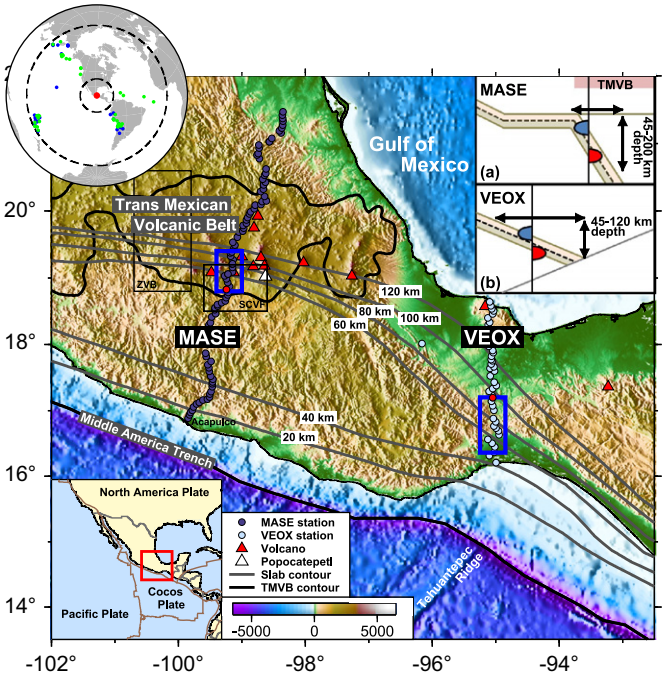


**Fig. 1.** Location of the MASE and VEOX lines in central and southern Mexico, respectively. The average distance between stations for both seismic lines is about 6 km. The regions of focus are shown by blue boxes. Two black boxes outline the Zitácuaro-Valle de Bravo (ZVB) and the Sierra Chichináutzin Volcanic Field (SCVF) in central Mexico (Cervantes and Wallace, 2003; Johnson et al., 2009). Gray lines depict isodepth contours of the subducted Cocos plate beneath the North American plate based on local seismicity and teleseismic receiver functions (Pérez-Campos et al., 2008; Kim et al., 2010, 2011; Melgar and Pérez-Campos, 2010). The upper-left inset illustrates teleseismic earthquake locations used in the analysis (MASE, 28 events: blue; VEOX, 45 events: green). The upper-right inset shows geometries of the subducted oceanic crust in central (a) and southern (b) Mexico, constrained by the receiver functions (Pérez-Campos et al., 2008; Kim et al., 2010, 2011, 2012; Melgar and Pérez-Campos, 2010).

dipping oceanic crust in central and southern Mexico from the RF amplitude inversion (Kim et al., 2010), we compare the differences in slab properties between central and southern Mexico, and discuss inferred relationships to the volcanic arc process in the overriding plate and overall plate boundary evolution in Mexico.

## 2. Observations

### 2.1. Data

We use teleseismic waveforms recorded from two passive seismic experiments in central and southern Mexico. Three-component broadband seismometers were deployed in two linear arrays (separated by $\sim$500 km) that are nearly perpendicular to the strike of the Middle America Trench (Fig. 1). The northern array (Meso-American Subduction Experiment, MASE) spanning from Acapulco at Pacific side across central Mexico (Fig. 1) was operational from 2005 and 2007 and consisted of 100 broadband seismometers. The southern array (Veracruz-Oaxaca (VEOX) line) in the Isthmus of Tehuantepec (Fig. 1) was operational from 2007 and 2008 and consisted of 45 broadband seismometers. This particular array geometry including a few permanent seismic stations from Servicio Sismológico Nacional (SSN) in Mexico provides dense station coverage to (1) investigate the dynamics of the young, shallowly dipping Cocos plate via seismic imaging, in particular their relation to mineral and fluid-phase reactions in the subducting crust and mantle wedge, and (2) build a dynamical model of the subduction process.

Teleseismic Ps waveforms from earthquakes with magnitude greater than 6.1 and epicentral distances between 30° and 90° (Fig. 1, upper-left inset) are collected from the MASE and VEOX and then band-passed from 0.01 to 1.0 Hz. For this study, 28 events recorded on eight stations above the TMVB in central Mexico from 06/2005 to 02/2007 and 43 events from 12 stations in southern Mexico from 08/2007 to 10/2008 are used to compute the RFs. We note that the first two VEOX stations near the Pacific coast (Fig. 1), which sample the Cocos oceanic crust at 35–45 km depth, are excluded in the analysis because their seismic recordings were heavily affected by frequent flooding events during the experiment. Individual waveform data recorded from the selected stations are first time-windowed to 90 s and rotated to radial and tangential coordinates. The radial component seismograms are then deconvolved with vertical component seismograms at each station to obtain radial RFs. The RF calculations are done in both frequency domain (Gaussian width factor of 2.5 and 5, and water level of 0.1, 0.01, and 0.001) (Langston, 1979; Ammon et al., 1990) and time domain (Gaussian parameter of 4 and maximum 100 picks or iterations) (Kikuchi and Kanamori, 1982; Ligorria and Ammon, 1999). The time domain deconvolution, in particular, is based on the least squares minimization of the difference between the observed horizontal component and the predicted signal generated by the convolution of an iteratively updated signal spike train and the vertical component seismogram (Kikuchi and Kanamori, 1982). The iterations can be repeated until a chosen percentage of the total energy has been removed, or until a user-specified iteration number has been reached. In this study, in order to ensure that the converted arrivals from the dipping oceanic crust are obtained, we set the maximum iteration to be 100 for the 90 s window. In comparison with the RFs processed in the frequency domain, the iterative deconvolution shows several desirable qualities, and thus for inversion, we only use the quality RF dataset from the iterative deconvolution in time domain for following reasons. The time domain deconvolution provides the highest resolution for sharply constraining the geometry of the slab beneath Mexico (Kim et al., 2010, 2011), and returns more stable results from noisy stations, especially those above the TMVB. Also, the high frequency content (0.01–1.0 Hz) in the data and iterative time domain deconvolution minimize waveform interference caused by the timing and amplitude variation due to slab dip and slowness. In addition, in each iteration, the quality of the deconvolution can be directly evaluated by comparing the detected phase energy before and after the deconvolution.

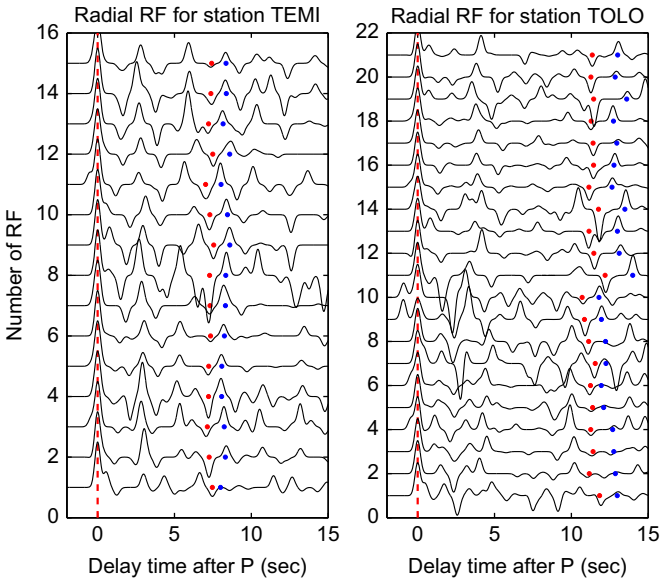


**Fig. 2.** Receiver functions for stations TEMI above the TMVB in central Mexico and TOLO in southern Mexico. The station locations are shown in Fig. 1 as red circles. Waveform from teleseismic events, as shown in Fig. 1 upper-left inset, are first filtered at 0.01–1.0 Hz and processed by the time domain deconvolution (Kikuchi and Kanamori, 1982; Ligorria and Ammon, 1999) with a Gaussian filter parameter of 4. The *P* arrival is indicated at 0 s as a red dotted line. Locations of the converted phases at top and bottom of the subducted oceanic crust are indicated as red and blue dots, respectively. These locations for central Mexico beneath the active arc are confirmed by the predicted arrivals from the synthetic seismograms based on the ray-based algorithm (Kim et al., 2012), and the locations for southern Mexico are by the predicted arrivals from the two-dimensional RF finite-difference modeling (Kim et al., 2011).

We then measure the amplitudes of the negative–positive pair in each RF, normalized by its P arrival, that are the converted phases at the top and bottom interfaces of the subducted crust (Fig. 2). The collection of the RF amplitudes for all the selected stations (Fig. 1) is used in the inversion which we describe in Section 3. Fewer stations and thus a smaller dataset for MASE above the TMVB reflects difficulties in picking phases corresponding to the top and bottom of the oceanic crust in the steeply dipping geometry (see Section 2.2). We also note that the seismic multiples in the teleseismic data recorded from both MASE and VEOX arrays are very weak in our high-frequency passband (Kim et al., 2010, 2011), and so it is difficult to clearly identify reverberated phases and measure timings of both forward conversions and reverberations to recover Vp/Vs of the subducted low-velocity oceanic crust as done by Audet et al. (2009) for Cascadia subduction zone. In particular, the reverberations at the steep interface ($>$ 50°) cause converted phases to travel over larger lateral offsets, and consequently are beyond the array (MacKenzie et al., 2010; Kim et al., 2012).

### 2.2. Geometries of the subducted Cocos oceanic crust in Mexico

The subducted Cocos plate beneath central Mexico, as imaged with both RFs and teleseismic migration (Bostock et al., 2001; Rondenay et al., 2005) from the MASE line, dips shallowly ($\sim$18°) near Acapulco on the Pacific coast and then tectonically underplates the continental crust for a distance of approximately

300 km from the Middle America Trench (Pérez-Campos et al., 2008; Kim et al., 2010, 2012). Although the estimate of the thickness slightly trades off with its velocity, the thickness of the oceanic crust is constrained at 7–8 km at the shallow-to-flat regime near the Pacific coast by the finite-difference modeling (Pérez-Campos et al., 2008; Kim et al., 2010) with a priori constraint of 5–7 km thick oceanic crust at the trench (Shor and Fisher, 1961). Among the flat subduction regions around the world, the subduction system in central Mexico is unique in a sense that the horizontal oceanic crust with normal oceanic crustal thickness is situated at a very shallow depth ($\sim$45 km) without mantle lithosphere or asthenosphere between the subducted oceanic lithosphere and the continental crust (Pérez-Campos et al., 2008; Kim et al., 2010, 2012).

Beyond the flat segment, the Cocos plate is imaged to be subducting steeply ($\sim 75^\circ$) underneath the active arc front of the TMVB (Husker and Davis, 2009; Kim et al., 2010, 2012). The top interface of the steeply dipping oceanic crust is clearly imaged in the migration image from the upgoing Ps phase (Kim et al., 2010, 2012) from teleseismic events which arrive obliquely incident to our 2-D station geometry. These images show a sharp boundary between gabbroic oceanic crust and surrounding peridotitic mantle from $\sim$45 km to 200 km at depth. The ability of the migration was tested using synthetic seismograms based on the ray-based algorithm (Frederiksen and Bostock, 2000), and the migration image from the synthetics showed that only Ps phase produces the conversion from the steep interface (Kim et al., 2012). The tomography also showed the steep slab which continues down to a depth of $\sim$ 500 km at a distance of 400 km from the trench (Husker and Davis, 2009). These seismic images of the steep slab beneath the arc support the slab rollback mode of the Cocos plate in central Mexico, which is also evidenced by the southeastward migration of TMVB volcanism since $\sim$20 Ma (Ferrari, 2004; Ferrari et al., 2011). In addition, an eastward migration pulse of magmatism originating beneath the Gulf of California at the time of the formation of Rivera Plate truncated the slab so that it only extends to 500 km depth today (Ferrari, 2004).

In contrast, the RF image across the VEOX line in southern Mexico (Fig. 1) shows the Cocos slab dipping $\sim 25^\circ$ to a depth of $\sim$120 km (Melgar and Pérez-Campos, 2010; Kim et al., 2011; Chen and Clayton, in review). Small azimuthal variations are observed in the RF image for the shallowly dipping Cocos slab, and smaller tangential RF amplitudes suggest that seismic anisotropy may be minor (Kim et al., 2011). Both the RF (Kim et al., 2011) and tomography images (Chen and Clayton, in review) reveal the presence of the southwest-dipping structure from Gulf of Mexico (denoted as Yucatán slab) with an opposite direction dip as the Cocos slab (approximate location shown in Fig. 1, inset (b)). Relocated seismicity (Castro Artola, 2010) follows the trend of the Yucatán slab starting at the intersection point with the Cocos slab ($\sim 120-150$ km depth) (Kim et al., 2011; Chen and Clayton, in review).

### 2.3. *Hydrous minerals in shallow-to-horizontal oceanic crust in central Mexico*

This analysis has been described fully in previous paper (Kim et al., 2010), and their results are briefly described here. The converted amplitudes from the top and bottom of the oceanic crust were used to estimate the mineral components of the oceanic crust as a function of depth ($\sim 20-45$ km) transitioning from shallow to flat geometry along the transect from Acapulco on Pacific coast to the southern end of the TMVB. The resultant S wave velocities in the shallowly dipping to flat, $4 \pm 1$ km thick, upper oceanic crust range between 2.3 and 3.4 km/s, and these velocities were directly compared with computed mineral phases such as chrysotile, (*c*-axis and randomly oriented) talc, antigorite, lizardite, and Fe-bearing phase A, and rocks such as gabbro, harzburgite, and pyroxenite (Kim et al., 2010). The velocities of the candidate mineral phases were computed at a depth 35 km and a range of temperatures (500–800°C) without the presence of a fluid (Kim et al., 2010). A low-pressure mineral phase such as talc (low-strength hydrous mineral) was considered a prime candidate for the anomalously low shear velocities inverted from the seismic data (Kim et al., 2010). Presence of such mechanically weak minerals can be important in lubricating and softening shear zones in the plate interface. Observed low S wave velocities and high Vp/Vs ratios in the upper oceanic crust are also related to localized seismic anisotropy predominantly caused by strain-induced crystallographic preferred orientation (CPO) developed in S–C mylonites (Song and Kim, 2012). The data for the lower oceanic crust, on the other hand, suggested the presence of unaltered oceanic crustal compositions (MORB-like) over dry-depleted mantle rock (Kim et al., 2010). High-pressure hydrous phases such as Fe-bearing phase A and depleted mantle rocks such as pyroxenite and harzburgite were characterized by higher S-wave velocities than the lower crustal data (Kim et al., 2010).

## 3. Bayesian inversion of receiver function amplitude

The inversion capability using the RF amplitudes was previously demonstrated based on the linearized Zoeppritz equation assuming small incidence angles, which was suitable for conversions along the portion of the shallowly dipping oceanic crust before steeply subducting beneath the TMVB (Kim et al., 2010). The amplitudes of the distinct negative/positive signature of the RF pulses converted from the top and bottom interfaces of the oceanic crust and their time separation were used to constrain the shear speed and density of the upper and lower oceanic crusts and the thickness, respectively. The initial negative pulse depends on the shear-speed and density variations of the top interface of the upper oceanic crust, while the following positive pulse depends on the contrast in these quantities across the bottom interface of the lower oceanic crust. In the inversion, Kim et al. (2010) used a single optimum reference model for P wave and S wave velocities and density, primarily constrained by the finite-difference modeling of the RFs, local velocity model by Valdes-Gonzalez and Meyer (1996), and waveform modeling of SP phase (Song et al., 2009), and inverted for absolute S wave velocities and densities rather than the perturbations. The inverted values were mapped in the 2-D strip of variations along the seismic line to properly account for the off-axis piercing points (Kim et al., 2010). As discussed in Kim et al. (2010), the measured conversion amplitudes have strong sensitivity to shear speed and weak sensitivity to density over the limited range in slowness ($p \sim 0.04-0.08$ s/km).

In this study, we implement Bayesian sampling in the inversion for shear speed and density of the upper and lower oceanic crusts, to first account for the uncertainty in the reference model for more steeply dipping geometries (Fig. 1, insets (a) and (b)). In particular, we do not have a well-constrained reference model that describes the structure beneath the TMVB in central Mexico (Fig. 1). The Bayesian sampling is a probabilistic approach that samples models in the solution space proportionally to how consistent the models are with data (likelihood), as well as with the prior information, and produces a distribution of possible models (posterior) for the inverse problem (Tarantola, 2005; Minson, 2010). The seismic parameters for the layer above and below the upper/lower oceanic crust are randomly generated from Gaussian distribution curves with given mean and standard deviation parameter. For the mean, we use a value 3% larger than the IASP91 Earth reference model (Kennett and Engdahl, 1991)

based on the tomographic model for central Mexico provided by Husker and Davis (2009). The standard deviation is set to 1 km/s. Trial and error shows that a larger range generates too many unphysical models. The Bayesian approach yields an estimate of the probability density function of all the possible input parameters, which can then be propagated through the forward model to determine the shear speeds and densities and their associated uncertainty distributions. We generate 10,000 models for each station to ensure a proper sampling of the posterior probability distribution.

For the inversion, we use Zoeppritz equation for sub-critical plane-wave transmission coefficient between two elastic half-spaces (Aki and Richards, 2002, p. 148):

$$T^{PS} = \frac{p\alpha}{2\cos j}\left[\left(1-2\beta^2p^2-2\beta^2\frac{\cos i}{\alpha}\frac{\cos j}{\beta}\right)\frac{\Delta\rho}{\rho} -4\beta^2\left(p^2+\frac{\cos i}{\alpha}\frac{\cos j}{\beta}\right)\frac{\Delta\beta}{\beta}\right], \quad (1)$$

where $p$ represents the ray parameter, $\alpha$ the P-wave velocity, $\beta$ the S-wave velocity, $\rho$ the density, and $i$ and $j$ the incident and transmitted angles, respectively. By considering the case with no conversions as a reference ray, the transmission coefficients $T^{PS}$ at the top and bottom of the oceanic crust can be effectively isolated and used in the inversion. The detailed analysis of the inversion procedure is described in Kim et al. (2010).

## 4. Results

### 4.1. Candidate phases

Fig. 3 shows the Vp/Vs as a function of shear wave velocities of candidate mineral phases such as amphibole, antigorite, lawsonite, zoisite, and pyroxene, and candidate rocks such as eclogite and gabbro, computed at different pressure ($P$)–temperature ($T$) conditions for central and southern Mexico. Predicted seismic velocities for each mineral phase are computed using elasticity data that have been experimentally determined (Table 1), and third-order finite strain theory (Duffy and Anderson, 1989) for $P$–$T$ conditions corresponding to different slab depths. The $P$–$T$ information at 45 km, 120 km, and 200 km is taken from a thermal model of the central Mexico subduction zone (Manea and Manea, 2011), and shown in Table 2. We note that elasticity data for some of the phases at high $P$–$T$ conditions are still lacking. In this case, we approximate these phases with reported values of other upper mantle phases (specified as 'assumed' in Table 1). The gabbroic rock is computed using the Voigt–Reuss–Hill (VRH) approximation on the combination of 50% plagioclase and 50% pyroxene (Mavko et al., 2003).

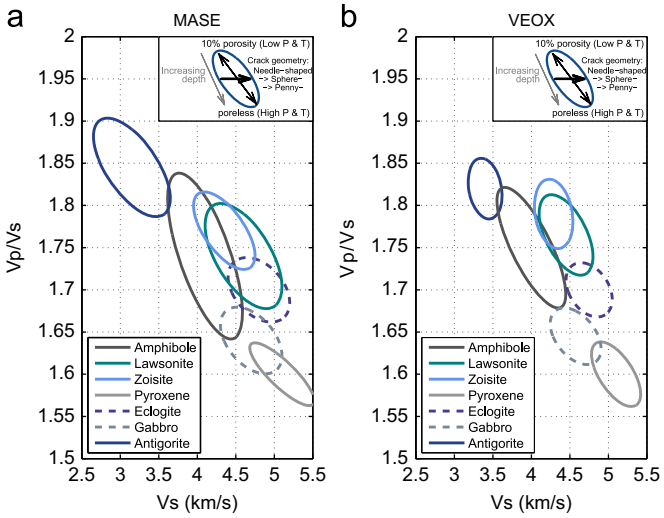


**Fig. 3.** Calculated Vp/Vs ratio versus Vs at depth ranges for (a) MASE from 45 km to 200 km and for (b) VEOX from 45 km to 120 km for candidate phases (amphibole, lawsonite, zoisite, pyroxene, eclogite, gabbro, and antigorite). The ellipses in solid and dotted lines represent candidate mantle mineral and rock properties, respectively. The elasticity data for the mineral phases and rocks used in these calculations are provided in Table 1, and the $P$–$T$ data in Table 2. The lower-right part in each ellipse represents poreless mineral or rock phases in high $P$ and $T$ conditions, and the upper-left portion represents the phases with various shape-crack, water-filled inclusions of maximum porosity 0.1 in low $P$ and $T$ conditions. Supplementary Fig. S1 shows how different crack geometry affects seismic velocities, and each ellipse in this figure and Supplementary Fig. S1 is drawn to encompass all velocities.

Based on the assumed $P$–$T$ conditions (Table 2), the elastic properties of candidate minerals and rocks are computed (1) without the presence of a fluid and (2) with needle-, sphere-, and penny-shaped, water-filled cracks with 10% porosity in each phase assemblage, calculated based on the Kuster and Toksöz formulation (Mavko et al., 2003). As shown in the insets of Fig. 3 and Supplementary Fig. S1, the major axis of each ellipse is primarily controlled by the $P$–$T$ conditions with different depths and the minor axis by various crack geometries (needle-, sphere-, and penny-shaped). The lower-right area of each ellipse corresponds to high $P$–$T$ values whereas the upper-right area represents low $P$–$T$ (Fig. 3). Calculated velocities from the needle-shaped, water-filled cracks from 0% to 10% porosity with different depths lie close to the area of the left part of the ellipse, and the velocities from the sphere-shaped with varying porosity lie close to the velocities from the needle-shaped, but characterized by higher Vs than those from the needle-shaped ones (Supplementary Fig. S1). On the other hand, the velocities from the penny-shaped ones lie close to the area of the right part of the ellipse (Supplementary Fig. S1). Each ellipse in Figs. 3 and 4, and Supplementary Figs. S1 and S2 includes the $P$–$T$ ranges, different crack geometries, and uncertainties in the elasticity data, as reported from the experimental results. In addition, we also consider elastic anisotropy of antigorite and texture observations in a natural serpentinite (Bezacier et al., 2010).

### 4.2. Hydrous minerals in dipping oceanic crust in Mexico

We determine major phases for the subducted oceanic crust underneath central and southern Mexico according to depths by comparing high-amplitude contours of our inverted seismic velocities with the computed properties of candidate phase assemblages, shown in Fig. 3 and Supplementary Fig. S1. Fig. 4a and b shows the Vp/Vs as a function of the inverted Vs based on the Bayesian sampling of 10,000 possible models for (a) MASE and (b) VEOX, respectively. The color contours in Fig. 4a and b show normalized amplitudes of probability distribution functions of the inverted Vs, and we only show high end of the amplitude range (from 0.8 to 1.0) to directly compare our results with the candidate phases with the smallest uncertainty. As we reduce the probability amplitudes, the error estimate increases and the distribution of the contours becomes broader. For both regions, the shallower portion of the oceanic crust corresponds to both higher Vp/Vs ratio and lower Vs, and the deeper portion corresponds to both lower Vp/Vs ratio and higher Vs (Supplementary Fig. S2). In general, contoured amplitude patterns for the inverted seismic velocities between upper and lower oceanic crusts for both regions are similar due to the fact that the input seismic parameters for the layer above/below the upper/lower oceanic crusts are not very different from each other. We also note that both regions contain seismic observations that do not fully match the candidate compositions explored here (Fig. 3, Supplementary Fig. S1). These regions are mostly characterized by low Vs and

**Table 1**
Densities, thermal expansion coefficients, elastic moduli, and their temperature and pressure derivatives for candidate phases.

| | $\rho_0$ (g/cm$^3$) | $\alpha_0$ ($10^{-5}$/K) | $K_0$ (GPa) | $G_0$ (GPa) | $\partial K_0/\partial T$ (GPa/K) | $\partial G_0/\partial T$ (GPa/K) | $\partial K_0/\partial P$ | $\partial G_0/\partial P$ |
|---|---|---|---|---|---|---|---|---|
| Lawsonite | 3.09[a] | 3.16[a] | 125.1[b] | 52.3[b] | −0.0179[b] | 0.0201[b] | 4.0[a] | 1.7[a] |
| Amphibole | 3.15[c] | 2.38[d] | 94.0[e] | 49.0[a] | −0.0154[a] | 0.0125[a] | 6.3[e] | 1.7[e] |
| Anorthite | 2.76[f] | 1.6[d] | 84.0[g] | 40.0[g] | −0.0154[a] | 0.0125[a] | 4.0[a] | 1.1[a] |
| Zoisite | 3.30[a] | 1.6[a] | 125.1[h] | 55.0[a] | −0.0125[h] | 0.0125[a] | 4.0[h] | 1.7[a] |
| Orthoenstatite | 3.196[i] | 3.2[a] | 108.5[j] | 77.9[j] | −0.0263[a] | 0.0136[a] | 8.5[k] | 1.6[j] |
| Eclogite | 3.50[c] | 3.2[a] | 135.3[l] | 74.38[l] | −0.0263[a] | 0.0136[a] | 8.5[a] | 1.6[a] |
| Antigorite | 2.62[m] | 3.4[m] | 67.9[m] | 38.5[m] | −0.0170[a] | −0.015[a] | 5.8[a] | 0.3[a] |

[a] Assumed.
[b] Schilling et al. (2002).
[c] Ringwood and Green (1966).
[d] Fei (1995).
[e] Comodi et al. (2010).
[f] Knittle (1995).
[g] Stixrude and Lithgow-Bertelloni (2005).
[h] Grevel et al. (2000).
[i] Jackson et al. (2007).
[j] Flesch et al. (1998).
[k] Angel and Jackson (2002).
[l] Anderson (1989).
[m] Bezacier et al. (2010).

**Table 2**
Pressure–temperature information from Manea and Manea (2011).

| Depth (km) | Pressure (GPa) | Temperature (°C) |
|---|---|---|
| 45 | 1.2 | 450 |
| 120 | 2.0 | 700 |
| 200 | 3.5 | 1000 |

high Vp/Vs exceeding 1.83 (Fig. 4). Preferentially oriented serpentinites can provide an explanation to some of these regions (Bezacier et al., 2010) (Fig. 4), but cannot be used to explain the full range of our observations. Other explanations could include free fluids, fabric development, as well as a lack of complete elasticity data for all candidate phases, including phase transitions and elastic anisotropy.

We note that density is not as good of an indicator to distinguish compositional models from this dataset because the inversion is more sensitive to the perturbation in shear velocities rather than density (Kim et al., 2010). The probability distributions of the inverted densities for both central and southern Mexico show rather broad distributions of values between 3200 and 3400 kg/m$^3$ without any distinct peak.

#### 4.2.1. Central Mexico

Similar peak patterns for the upper and lower oceanic crusts at depths (45–200 km) in central Mexico likely mean that the steeply dipping oceanic crust becomes more homogeneous in composition as the depth increases (Fig. 4a). Observed seismic velocities from ~60 to 100 km depth in the upper and lower oceanic crusts beneath central Mexico correspond to computed velocities of hydrous minerals such as zoisite and lawsonite (~0–5% porosity) (Fig. 4a). Based on this seismic observation, we cannot distinguish whether two phases coexist or not, due to their similar velocities at the depth of ~60–100 km. The data points for depth shallower than ~60 km correspond to low Vs (3.8–4.3 km/s) and high Vp/Vs (1.83–2.0). As Kim et al. (2010) suggested from their analysis for the region south of our study area, a combination of added pore fluid pressure and pervasive presence of hydrous minerals such as talc may affect seismic velocities. Also, seismic anisotropy from the preferentially oriented serpentinites (Bezacier et al., 2010) may explain such anomalous data points.

As shown in Fig. 4a, the candidate phase assemblages which explain our deeper-depth (> ~100 km) data are gabbro (~0–4% porosity) and eclogite (~6% porosity). Observed dominant gabbroic phase at deeper depth (> ~100 km) is supported by the seismic image (Kim et al., 2012) showing the sharp boundary between the top interface of the steeply subducting slab and the peridotitic mantle, which extends down to a depth of 200 km although the image does not show the oceanic Moho (bottom of the oceanic crust) due to the low frequency range in the analysis (0.03–0.3 Hz) and resolution limit (Rondenay et al., 2005; MacKenzie et al., 2010). It is generally understood that large amount of fluid is expelled from the downgoing hydrated crust as it undergoes subduction-zone metamorphism with increasing $P$ and $T$, and the degree of dehydration strongly controls the reflectivity at the top and bottom of the oceanic crust (Kawakatsu and Watada, 2007). Such slab dehydration is suggested to be a reason for weaker or absence of gabbroic crust in the upper-most oceanic mantle in the teleseismic migration images (Bostock et al., 2002; Abers et al., 2009). Depending on different thermal state of the subduction system, the conversion from gabbroic to anhydrous eclogitic crust due to metamorphism occurs at different depths, and the eclogitic crust is seismically indistinguishable from the mantle peridotite (Bostock et al., 2002; Kawakatsu and Watada, 2007; Abers et al., 2009). Our seismic data for central Mexico indicate that eclogite is present after the depth of 100 km, although it is difficult to disentangle the gabbroic signature (Fig. 4a). In particular, the eclogitization underneath the TMVB is in good agreement with the slab rollback process evidenced by the southward migration of the volcanism (Ferrari et al., 2001). Overall, the deeper-depth data can be explained by mineral-bound $H_2O$ within the subducted oceanic crust.

The release of $H_2O$ from lawsonite and/or zoisite above 100 km depth by slab dewatering process could be in the form of a fluid phase and/or could lower the melting temperature of surrounding phases, where either scenario correlates well with arc volcanism. A large extent and heterogeneous volcanic signatures in the TMVB have been previously suggested to be due to a change in subduction dynamics from normal subduction geometry to the current configuration since ~15 Ma in central Mexico (Blatter et al., 2007; Manea and Manea, 2011). One of the puzzling aspects of

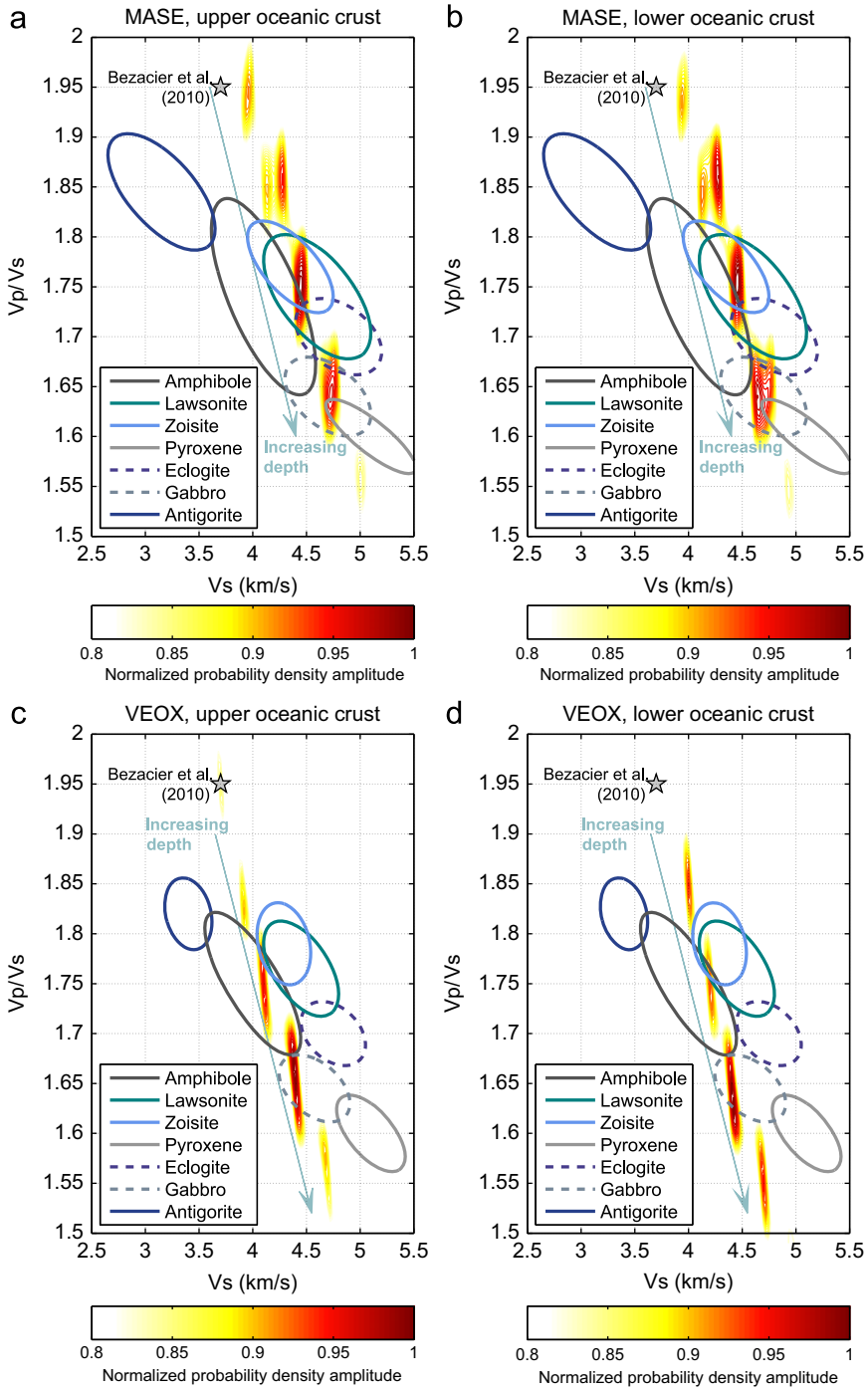


**Fig. 4.** Calculated Vp/Vs ratio versus Vs at depth ranges for (a) MASE from 45 km to 200 km and for (b) VEOX from 45 km to 120 km. The Vs are computed for 10,000 one-dimensional Earth models, which are generated by randomly varying the velocities and densities within a prescribed range. The colorbar represents normalized probability amplitudes corresponding to all the possible Vs as contours, and we only show high end of the amplitude range in warm colors. The ellipses in solid and dotted lines (both in cold colors) represent candidate mantle mineral and rock properties, respectively (see Fig. 3 and Supplementary Fig. S1). The lower-right part in each ellipse represents poreless mineral or rock phases in high *P* and *T* conditions, and the upper-left portion represents the phases with various shape-crack, water-filled inclusions of maximum porosity 0.1 in low *P* and *T* conditions. The elasticity data for the phases and rock used in these calculations are provided in Table 1 and the *P*–*T* data in Table 2. The data point shown as a star indicates a value computed for Vs at a 30° incidence angle between the seismic ray path and foliation plane of Cuba serpentinite at room *P* and *T* (Bezacier et al., 2010). The shallow depth part of the oceanic crust corresponds to the higher Vp/Vs ratio and lower Vs, and the deeper depth part corresponds to the lower Vp/Vs ratio and higher Vs (Supplementary Fig. S2).

the TMVB volcanism is that compositionally contrasting suites of rocks have erupted all across the arc since the middle-late Miocene (Gómez-Tuena et al., 2007, 2008; Straub et al., 2008, 2011). In particular, the data for $H_2O$ and trace elements in melt inclusion from high-Mg basalts in the arc-front volcanoes (less than 50 km apart) in Quaternary Sierra Chichináutzin Volcanic Field (SCVF) (Fig. 1) suggest significant variability in the composition of $H_2O$-rich subduction compositions that are added to the mantle wedge (Cervantes and Wallace, 2003). Whereas, the generation mechanism of the Quaternary volcanism in the Zitácuaro-Valle de Bravo (ZVB), situated east of the SCVF and 280–330 km from the trench (Fig. 1), is mostly due to partial

melting of depleted mantle peridotite and is strongly influenced by subduction-related fluids (Blatter et al., 2007). The Cocos plate is steeply subducting beneath two volcanic regions (SCVF and ZVB), and the magmatic $H_2O$ contents in the monogenetic volcanoes in these regions range between 2.0 and 6.0 wt% (Johnson et al., 2009).

The active slab dewatering process inferred from our inverted data may also well correlate with highly attenuating region in the overlying mantle wedge beneath the TMVB at a depth of 80–120 km (Chen and Clayton, 2009). This highly attenuated area was previously suggested to be related to fluids and partial melts produced in the subduction process (Chen and Clayton, 2009). Furthermore, at a depth of 20–40 km, the slab dewatering process followed by the slab rollback was seismically evidenced as a low-resistivity anomaly at the lower continental crust directly beneath the entire arc (Jödicke et al., 2006). This anomaly has also been shown as high seismic attenuation (Chen and Clayton, 2009) and low shear wave velocities (Iglesias et al., 2010).

#### 4.2.2. Southern Mexico

Similar to the central Mexico case, similar peak locations for the upper and lower oceanic crusts are observed at depths (45–120 km) beneath southern Mexico (Fig. 4b). However, high probability amplitudes are distributed differently with depth, which may suggest that mineralogical properties for the upper and lower crusts are different (Fig. 4b). Also, the observed contours for the probability amplitudes are tightly bounded between 0.8 and 1.0 compared to those for central Mexico, indicating smaller uncertainty in the data based on more sampling points (i.e., more station-and-event pairs) and higher accuracy in picking the phases (Fig. 4b). Previous two-dimensional finite-difference modeling suggested that two low-velocity layers (upper crustal velocity being $\sim 20-25\%$ slower than the lower one) are required to explain the observed negative and positive RF pulse heights and timing of the pulses (Kim et al., 2011). This also strongly suggests that the compositions of two layers are different.

In southern Mexico, the dominant mineral phase is observed to be amphibole ($< \sim 5\%$ porosity) in shallowly dipping upper oceanic crust (Fig. 4b). The amphibole-dominated mineralogy in the oceanic crust in the subduction zone has been commonly known, and its presence suggests that it can be an important host for $H_2O$ (Poli and Schmidt, 1995). The amphibole-bearing oceanic crustal assemblage is also seen in central Andes where the Nazca plate is subducting under the South American continent (ANCORP Working Group, 2003). A strong dipping (Nazca) reflector was previously linked to the subducting oceanic crust down to a depth of $\sim 85$ km, which corresponds to the lower stability limit of amphibole minerals in mafic rocks (ANCORP Working Group, 2003). The observation of this dominant amphibole composition in the upper crust beneath southern Mexico is quite different from the central Mexico case for the shallow-to-flat slab region at depths ranging from 20 to 45 km (Kim et al., 2010). The difference in the compositions of the upper oceanic crust beneath two different regions clearly reflects the difference in slab geometry. Furthermore, the "normal" mineral assemblage in the dipping oceanic crust beneath southern Mexico based on our seismic observation makes the case in central Mexico unique and unusual. The origin of the flat subduction in central Mexico is not clear (Skinner and Clayton, 2010), and the presence of hydrous mantle mineral, talc, in the upper oceanic crust beneath central Mexico may provide a clue to complicated slab dynamics in the past, which lead to the current configuration.

Lower crustal data, on the other hand, suggest dominant gabbroic compositions ($\sim 10\%$ porosity) in southern Mexico (Fig. 4b). This is consistent with the previous observation that Kim et al. (2010) made for central Mexico in the shallow-to-flat slab region. Based on this analysis, we note that the gabbro-to-eclogite transformation has not occurred in southern Mexico. As a comparison, Cascadia, the youngest and warmest slab in the world (Hyndman and Wang, 1993), has the formation of nearly anhydrous eclogite at 80–90 km (Hacker et al., 2003b).

## 5. Conclusions

We apply the inversion technique using the receiver function (RF) amplitudes to obtain the S wave velocity (Vs) and density of the steeply and shallowly dipping Cocos oceanic crust in central and southern Mexico, respectively. Because inverted Vs and density are highly sensitive to the input reference model, we approach the inverse problem from a Bayesian perspective, allowing us to completely characterize the model parameter space by computing allowable models instead of seeking a single optimum model. The resulting probability distribution of the inverted Vs is then used to provide tighter constraints on the physical properties of the subducted Cocos oceanic crust and to explain the difference in slab geometries between central and southern Mexico by using available mineral physics data.

In central Mexico, the compositions of the more steeply subducting oceanic crust include hydrous mantle mineral phases, such as lawsonite and zoisite, at 60–100 km depth; the eclogitization occurs at $\sim 100$ km depth underneath the Trans-Mexican Volcanic Belt (TMVB). This result supports the subduction-related arc volcanism at the TMVB directly above the Cocos slab as well as the slab rollback. In particular, the release of $H_2O$ from lawsonite and zoisite by slab dehydration could be in the form of a fluid phase and/or could lower the melting temperature of surrounding phases, where either scenario correlates well with arc volcanism. On the other hand, the dominant mineral phase in the upper oceanic crust of southern Mexico is suggested to be amphibole on top of unaltered gabbroic oceanic crust. However, we note that both regions contain seismic observations that do not fully match the candidate compositions explored in this analysis. These regions are mostly characterized by low Vs and high Vp/Vs exceeding 1.83, and seismic anisotropy from the preferentially oriented serpentinites (Bezacier et al., 2010) may explain such anomalous data points. Free fluids could provide an explanation to our seismic observations that do not intersect our compositional models, but require very low-permeability be maintained over the entire 200 km flat portion of the slab. Other explanations could include a lack of complete elasticity data for all candidate phases, including phase transitions and elastic anisotropy.

## Acknowledgment

This study was supported by the Gordon and Betty Moore Foundation through the Tectonics Observatory at California Institute of Technology (Contribution number 176) and NSF award EAR 0609707. We thank Xyoli Pérez-Campos, Arturo Iglesias, and others at the Universidad Nacional Autónoma de México for deploying and maintaining the MASE and VEOX lines. We thank Joann Stock, Michael Gurnis, and Victor Tsai from California Institute of Technology for suggestions, and Ting Chen for providing slab contour lines for Mexican subduction zone. Finally, we thank Editor Peter Shearer and two anonymous reviewers for helpful comments which improved the manuscript.

## Appendix A. Supplementary data

Supplementary data associated with this article can be found in the online version at http://dx.doi.org.10.1016/j.epsl.2012.06.001.

## References


Abers, G.A., 2000. Hydrated subducted crust at 100–250 km depth. Earth Planet. Sci. Lett. 176, 323–330.

Abers, G.A., MacKenzie, L.S., Rondenay, S., Zhang, Z., Wech, A.G., Creager, K.C., 2009. Imaging the source region of Cascadia tremor and intermediate-depth earthquakes. Geology 37, 1119–1122.

Aki, K., Richards, P.G., 2002. Quantitative Seismology, 2nd ed. University Science Books, Sausalito, California.

Ammon, C.J., Randall, G.E., Zandt, G., 1990. On the nonuniqueness of receiver function inversions. J. Geophys. Res. 95 (B10), 15303–15318.

ANCORP Working Group, 2003. Seismic imaging of a convergent continental margin and plateau in the central andes (andean continental research project 1996 (ancorp'96)). J. Geophys. Res. 108 (B7).

Anderson, D.L., 1989. Theory of the Earth. Blackwell Scientific Publications.

Angel, R.J., Jackson, J.M., 2002. Elasticity and equation of state orthoenstatite, $MgSiOi_3$. Am. Mineral. 87, 558–561.

Audet, P., Bostock, M.G., Boyarko, D.C., Brudzinski, M.R., Allen, R.M., 2010. Slab morphology in the Cascadia fore arc and its relation to episodic tremor and slip. J. Geophys. Res. 115 (B00A16).

Audet, P., Bostock, M.G., Christensen, N.I., Peacock, S.M., 2009. Seismic evidence for overpressured subducted oceanic crust and megathrust fault sealing. Nature 457, 76–78.

Bach, W., Früh-Green, G.L., 2010. Alteration of the oceanic lithosphere and implications for seafloor processes. Elements 6, 173–178, http://dx.doi.org/10.2113/gselements.6.3.173.

Bezacier, L., Reynard, B., Bass, J.D., Sanchez-Valle, C., Van de Moortèle, B., 2010. Elasticity of antigorite, seismic detection of serpentinites, and anisotropy in subduction zones. Earth Planet. Sci. Lett. 289, 198–208, http://dx.doi.org/10.1016/j.epsl.2009.11.009.

Blatter, D.L., Lang Farmer, G., Carmichael, I.S.E., 2007. A north–south transect across the central Mexican volcanic belt at $\sim 100^{\circ}$W: spatial distribution, petrological, geochemical, and isotopic characteristics of Quaternary volcanism. J. Petrol. 48 (5), 901–950, http://dx.doi.org/10.1093/petrology/egm006.

Bostock, M.G., Rondenay, S., Shragge, J., 2001. Multiparameter two-dimensional inversion of scattered teleseismic body waves 1. Theory for oblique incidence. J. Geophys. Res. 106, 30771–30782.

Bostock, M.G., Hyndman, R.D., Rondenay, S., Peacock, S.M., 2002. An inverted continental Moho and the serpentinization of the forearc mantle. Nature 417, 536–538.

Castro Artola, O.A., 2010. Caracterización de la geometría de la zona benioff con una red densa de banda ancha en el istmo de Tehuantepec. B.A. Thesis, UNAM.

Cervantes, P., Wallace, P.J., 2003. Role of $H_2O$ in subduction-zone magmatism: new insights from melt inclusions in high-Mg basalts from central Mexico. Geology 31, 235–238.

Chen, T., Clayton, R.W., 2009. Seismic attenuation structure in central Mexico: image of a focused high-attenuation zone in the mantle wedge. J. Geophys. Res. 114 (B07304)http://dx.doi.org/10.1029/2008JB005964.

Chen, T., Clayton, R.W. Structure of central and southern Mexico from velocity and attenuation tomography, J. Geophys. Res., in review.

Christensen, N.I., 1984. Pore pressure and oceanic crustal seismic structure. Geophys. J. R. Astron. Soc. 79, 411–423.

Comodi, P., Ballaran, T.B., Zanazzi, P.F., Capalbo, C., Zanetti, A., Nazzareni, S., 2010. The effect of oxo-component on the high-pressure behavior of amphiboles. Am. Mineral. 95, 1042–1051.

Contreras-Reyes, E., Grevemeyer, I., Flueh, E.R., Scherwath, M., Heesemann, M., 2007. Alteration of the subducting oceanic lithosphere at the southern central Chile trench-outer rise. Geochem. Geophys. Geosyst. 8 (7), Q07003, http://dx.doi.org/10.1029/2007GC001632.

Currie, C.A., Hyndman, R.D., Wang, K., Kostoglodov, V., 2002. Thermal models of the Mexico subduction zone: implications for the megathrust seismogenic zone. J. Geophys. Res. 107 (B12).

Duffy, T.S., Anderson, D.L., 1989. Seismic velocities in mantle minerals and the mineralogy of the upper mantle. J. Geophys. Res. 94 (B2), 1895–1912.

Fei, Y., 1995. Thermal expansion. In: Ahrens, T.J. (Ed.), Mineral Physics and Crystallography: A Handbook of Physical Constants. American Geophysical Union, Washington, DC, pp. 29–44.

Ferrari, L., 2004. Slab detachment control on mafic volcanic pulse and mantle heterogeneity in central Mexico. Geology 32 (1), 77–80.

Ferrari, L., Petrone, C.M., Francalanci, L., 2001. Generation of oceanic-island basalt-type volcanism in the western Trans-Mexican volcanic belt by slab rollback, asthenosphere infiltration, and variable flux melting. Geology 29 (6), 507–510.

Ferrari, L., Orozco-Esquivel, T., Manea, V., Manea, M., 2011. The dynamic history of the Trans-Mexican Volcanic Belt and the Mexico Subduction zone. Tectonophysics 522–523 (5), 122–149, http://dx.doi.org/10.1016/j.tecto.2011.09.018.

Ferris, A., Abers, G.A., Christensen, D.H., Veenstra, E., 2003. High resolution image of the subducted Pacific (?) plate beneath central Alaska, 50–150 km depth. Earth Planet. Sci. Lett. 214, 575–588.

Flesch, L.M., Baosheng, L., Liebermann, R.C., 1998. Sound velocities of polycrystalline $MgSiOi_3$-orthopyroxene to 10 GPa at room temperature. Am. Mineral. 83, 444–450.

Franco, S.I., Kostoglodov, V., Larson, K.M., Manea, V.C., Manea, M., Santiago, J.A., 2005. Propagation of the 2001–2002 silent earthquake and interplate coupling in the Oaxaca subduction zone. Earth Planets Space 57, 973–985.

Frederiksen, A.W., Bostock, M.G., 2000. Modeling teleseismic waves in dipping anisotropic structures. Geophys. J. Int. 143, 401–412.

Gómez-Tuena, A., Langmuir, C.H., Goldstein, S.L., Straub, S.M., Ortega-Gutiérrez, F., 2007. Geochemical evidence for slab melting in the Trans-Mexican Volcanic Belt. J. Petrol. 48 (3), 537–562, http://dx.doi.org/10.1093/petrology/eg1071.

Gómez-Tuena, A., Mori, L., Rincon-Herrera, N.E., Ortega-Gutiérrez, F., Sole, J., Iriondo, A., 2008. The origin of a primitive trondhjemite from the Trans-Mexican volcanic belt and its implications for the construction of a modern continental arc. Geology 36, 471–474, http://dx.doi.org/10.1130/G24687A.1.

Grevel, K.-D., Nowlan, E.U., Fasshauer, D.W., Burchard, M., 2000. In situ X-ray diffraction investigation of lawsonite and zoisite at high pressures and temperatures. Am. Mineral. 85, 206–216.

Hacker, B.R., Abers, G.A., Peacock, S.M., 2003a. Subduction factory 1. Theoretical mineralogy, densities, seismic wave speeds, and $H_2O$ contents. J. Geophys. Res. 108.

Hacker, B.R., Peacock, S.M., Abers, G.A., Holloway, S.D., 2003b. Subduction factory 2. Are intermediate-depth earthquakes in subducting slabs linked to metamorphic dehydration reactions? J. Geophys. Res. 108 (B1).

Husker, A., Davis, P.M., 2009. Tomography and thermal state of the Cocos plate subduction beneath Mexico City. J. Geophys. Res. 114 (B04306), 1–15.

Hyndman, R.D., Wang, K., 1993. Thermal constraints on the zone of possible major thrust earthquake failure on the Cascadia margin. J. Geophys. Res. 98, 2039–2060.

Iglesias, A., Clayton, R.W., Pérez-Campos, X., Singh, S.K., Pacheco, J., Garcia, D., Valdes-Gonzalez, C., 2010. S-wave velocity structure below central Mexico using high-resolution surface wave tomography. J. Geophys. Res. 115 (B06307)http://dx.doi.org/10.1029/2009JB006332.

Jackson, J.M., Sinogeikin, S.V., Bass, J.D., 2007. Sound velocities and single-crystal elasticity of orthoenstatite to 1073 K at ambient pressure. Phys. Earth Planet. Inter. 161, 1–12.

Jacobsen, S.D., van der Lee, S., 2006. Earth's Deep Water Cycle. American Geophysical Union, Washington, DC.

Johnson, E.R., Wallace, P.J., Granados, H.D., Manea, V.C., Kent, A.J.R., Bindeman, I.N., Donegan, C.S., 2009. Subduction-related volatile recycling and magma generation beneath central Mexico: insights from melt inclusions, oxygen isotopes and geodynamic models. J. Petrol. 50 (9), 1729–1764.

Jödicke, H., Jording, A., Ferrari, L., Arzate, J., Mezger, K., Rüpke, L., 2006. Fluid release from the subducted Cocos plate and partial melting of the crust deduced from magnetotelluric studies in southern Mexico: implications for the generation of volcanism and subduction dynamics. J. Geophys. Res. 111 (B08102)http://dx.doi.org/10.1029/2005JB003739.

Kato, A., Iidaka, T., Ikuta, R., Yoshida, Y., Katsumata, K., Iwasaki, T., Sakai, S., Thurber, C., Tsumura, N., Yamaoka, K., Watanabe, T., Kunitomo, T., Yamazaki, F., Okubo, M., Suzuki, S., Hirata, N., 2010. Variations of fluid pressure within the subducting oceanic crust and slow earthquakes. Geophys. Res. Lett. 37 (L14310)http://dx.doi.org/10.1029/2010GL043723.

Kawakatsu, H., Watada, S., 2007. Seismic evidence for deep-water transportation in the mantle. Science 316, 1468–1471.

Kennett, B.L.N., Engdahl, E.R., 1991. Traveltimes for global earthquake location and phase identification. Geophys. J. Int. 105 (2), 429–465.

Kikuchi, M., Kanamori, H., 1982. Inversion of complex body waves. Bull. Seism. Soc. Am. 72 (3), 491–506.

Kim, Y., Clayton, R.W., Jackson, J.M., 2010. Geometry and seismic properties of the subducting Cocos plate in central Mexico. J. Geophys. Res. 115 (B06310).

Kim, Y., Clayton, R.W., Keppie, F., 2011. Evidence of a collision between the Yucatán Block and Mexico in the Miocene. Geophys. J. Int. 187, 989–1000.

Kim, Y., Miller, M.S., Pearce, F., Clayton, R.W., 2012. Seismic imaging of the Cocos plate subduction zone system in central Mexico, Geochem. Geophys. Geosyst. 13, http://dx.doi.org/10.1029/2012GC004033.

Knittle, E., 1995. Static compression measurements of equations of state. In: Ahrens, T.J. (Ed.), Mineral Physics and Crystallography: A Handbook of Physical Constants. American Geophysical Union, Washington, DC, pp. 98–143.

Kostoglodov, V., Husker, A., Shapiro, N.M., Payero, J.S., Campillo, M., Cotte, N., Clayton, R., 2010. The 2006 slow slip event and nonvolcanic tremor in the Mexican subduction zone. Geophys. Res. Lett. 37 (L24301).

Langston, C.A., 1979. Structure under Mount Rainier, Washington, inferred from teleseismic body waves. J. Geophys. Res. 84, 4749–4762.

Larson, K., Kostoglodov, V., Miyazaki, S., Santiago, J.A.S., 2007. The 2006 aseismic slow slip event in Guerrero, Mexico: new results from GPS. Geophys. Res. Lett. 34 (L13309).

Ligorria, J.P., Ammon, C.J., 1999. Iterative deconvolution and receiver-function estimation. Bull. Seism. Soc. Am. 89 (5), 1395–1400.

MacKenzie, L.S., Abers, G.A., Rondenay, S., Fischer, K.M., 2010. Imaging a steeply dipping subducting slab in Southern Central America. Earth Planet. Sci. Lett. 296 http://dx.doi.org/10.1016/j.epsl.2010.05.033.

Mainprice, D., IIdefonse, B., 2009. Subduction Zone Geodynamics. Springer, pp. 63–84.

Manea, V.C., Manea, M., 2011. Flat-slab thermal structure and evolution beneath Central Mexico. Pure Appl. Geophys. 168, 1475–1487, http://dx.doi.org/10.1007/s00024-010-0207-9.
Maruyama, S., Okamoto, K., 2007. Water transportation from the subducting slab into the mantle transition zone. Gondwana Res. 11, 148–165.
Mavko, G., Mukerji, T., Dvorkin, J., 2003. The Rock Physics Handbook: Tools for Seismic Analysis of Porous Media. Cambridge University Press, Cambridge, UK.
Melgar, D., Pérez-Campos, X., 2010. Imaging the Moho and subducted oceanic crust at the Isthmus of Tehuantepec, Mexico, from receiver functions. Pure Appl. Geophys. 168, 1449–1460.
Minson, S., 2010. A Bayesian Approach to Earthquake Source Studies. Ph.d. Thesis, California Institute of Technology, Pasadena, California.
Morán-Zenteno, D.J., Cerca, M., Keppie, J.D., 2007. The Cenozoic tectonic and magmatic evolution of southwestern Mexico: advances and problem interpretation. Spec. Pap. Geol. Soc. Am. 422, 71–91.
Nicholson, T., Bostock, M.G., Cassidy, J.F., 2005. New constraints on subduction zone structure in northern Cascadia. Geophys. J. Int. 161, 849–859.
Nieto-Samaniego, A.F., Alaniz-Álvarez, A.S., Silva-Romo, G., Eguiza-Castro, M.H., Mendoza-Rosales, C., 2006. Latest Cretaceous to Miocene deformation events in the eastern Sierra Madre del Sur, Mexico, inferred from the geometry and age of major structures. Geol. Soc. Am. Bull. 118, 238–252.
Payero, J.S., Kostoglodov, V., Shapiro, N., Mikumo, T., Iglesias, A., Pérez-Campos, X., Clayton, R.W., 2008. Nonvolcanic tremor observed in the Mexican subduction zone. Geophys. Res. Lett. 35 (L07305).
Peacock, S.M., Christensen, N.I., Bostock, M., Audet, P., 2011. High pore pressures and porosity at 35 km depth in the Cascadia subduction zone. Geology 39 (5), 471–474.
Pérez-Campos, X., Kim, Y., Husker, A., Davis, P.M., Clayton, R.W., Iglesias, A., Pacheco, J.F., Singh, S.K., Manea, V.C., Gurnis, M., 2008. Horizontal subduction and truncation of the Cocos Plate beneath central Mexico. Geophys. Res. Lett. 35 (L18303).
Poli, S., Schmidt, M.W., 1995. $H_2O$ transport and release in subduction zones: experimental constraints on basaltic and andesitic systems. J. Geophys. Res. 100, 22299–22314.
Radiguet, M., Cotton, F., Vergnolle, M., Campillo, M., Valette, B., Kostoglodov, V., Cotte, V., 2011. Spatial and temporal evolution of a long term slow slip event: the 2006 Guerrero Slow Slip Event. Geophys. J. Int. 184, 816–828, http://dx.doi.org/10.1111/j.1365-246X.2010.04866.x.
Ronero, C.R., Phipps Morgan, J., Mcintosh, K., Reichert, C., 2003. Bending-related faulting and mantle serpentinization at the Middle America Trench. Nature 425, 367–372.
Ringwood, A.E., Green, D.H., 1966. An experimental investigation of the Gabbro–Eclogite transformation and some geophysical implications. Tectonophysics 3 (5), 383–427.
Rondenay, S., Bostock, M.G., Fischer, K.M., 2005. Multichannel inversion of scattered teleseismic body waves: practical considerations and applicability. In: Levander, A., Nolet, G. (Eds.), Seismic Earth: Array Analysis of Broadband Seismograms. American Geophysical Union Geophysical Monograph, vol. 157; 2005, pp. 187–203.
Shelly, D.R., Beroza, G.C., Ide, S., Nakamula, S., 2006. Low-frequency earthquakes in Shikoku, Japan, and their relationship to episodic tremor and slip. Nature 442, 795–797.
Schilling, F.R., Sinogeikin, S.V., Bass, J.D., 2002. Single-crystal elastic properties of lawsonite and their variation with temperature. Phys. Earth Planet. Inter. 136, 107–118.
Shor Jr., G.G., Fisher, R.L., 1961. Middle America trench: seismic refraction studies. Geol. Soc. Am. Bull. 72, 721–730.
Skinner, S.M., Clayton, R.W., 2010. An evaluation of proposed mechanisms of slab flattening in central Mexico. Pure Appl. Geophys. http://dx.doi.org/10.1007/s00024-010-0200-3.
Song, T.A., Helmberger, D.V., Brudzinski, M.R., Clayton, R.W., Davis, P., Pérez-Campos, X., Singh, S.K., 2009. Subducting slab ultra-slow velocity layer coincident with silent earthquake in southern Mexico. Science 324, 502–506.
Song, T.A., Kim, Y., 2012. Localized seismic anisotropy associated with long-term slow-slip events beneath southern Mexico. Geophys. Res. Lett. 39 (L09308)http://dx.doi.org/10.1029/2012GL051324.
Straub, S.M., LaGatta, A.B., Martin-Del Pozzo, A.L., Langmuir, C.H., 2008. Evidence from high Ni olivines for a hybridized peridotite/pyroxenite source for orogenic andesites from the central Mexican Volcanic Belt. Geochem. Geophys. Geosyst. 9 (Q03007)http://dx.doi.org/10.1029/2007GC001583.
Straub, S.M., Gomez-Tuena, A., Stuart, F.M., Zellmer, G.F., Espinasa-Perena, R., Cai, Y., Iizuka, Y., 2011. Formation of hybrid arc andesites beneath thick continental crust. Earth Planet. Sci. Lett. 303, 337–347, http://dx.doi.org/10.1016/j.epsl.2011.01.013.
Stixrude, L., Lithgow-Bertelloni, C., 2005. Mineralogy and elasticity of the oceanic upper mantle: origin of the low-velocity zone. J. Geophys. Res. 110 (B03204)http://dx.doi.org/10.1029/2004JB002965.
Tarantola, A., 2005. Inverse Problem Theory and Methods for Model Parameter Estimation. Society for Industrial and Applied Mathematics, Philadelphia, PA, US.
Tsuji, Y., Nakajima, J., Hasegawa, A., 2008. Tomographic evidence for hydrated oceanic crust of the Pacific slab beneath northeastern Japan: implications for water transportation in subduction zones. Geophys. Res. Lett. 35.
Valdes-Gonzalez, C., Meyer, R.P., 1996. Seismic structure between the Pacific coast and Mexico City from the Petatlan earthquake (Ms=7.6) aftershocks. Geofis. Int. 35, 4377–4401.
Vergnolle, M., Walpersdorf, A., Kostoglodov, V., Tregoning, P., Santiago, J.A., Cotte, N., Franco, S.I., 2010. Slow slip events in Mexico revised from the processing of 11 year GPS observations. J. Geophys. Res. 115 (B08403).
Yuan, X., Sobolev, S.V., Kind, R., Oncken, O., Bock, G., Asch, G., Schurr, B., Graeber, F., Rudloff, A., Hanka, W., Wylegalla, K., Tibi, R., Haberland, C., Rietbrock, A., Giese, P., Wigger, P., Röwer, P., Zandt, G., Beck, S., Wallace, T., Pardo, M., Comte, D., 2000. Subduction and collision processes in the Central Andes constrained by converted seismic phases. Nature 408, 958–961.